

## Wide-Field Survey Reveals the Variable Sky

Steve B. Howell (NOAO) & Mark Huber (Lawrence Livermore National Laboratory)

We are entering an era of high interest in the variability of astronomical objects. Modern efforts in this area must not only optimize how data are collected, but also how they are stored and disseminated for most effective use—temporal information is often gleaned in hindsight, by looking back at past behavior, once interest in an object is triggered. In this article, we describe a large imaging survey with variability investigations as its primary goal.

The Faint Sky Variability Survey (FSVS) covers approximately 23 square degrees using B, V, I images. The survey was proposed by Co-Principal Investigators Jan van Paradijs and Steve Howell, et al., in response to the original call for survey proposals using the wide-field camera on the Isaac Newton Telescope (INT). The INT is part of a group of telescopes located at the Roque de Los Muchachos Observatory in La Palma, Spain. The proposal was one of six accepted, and the only one dedicated to galactic science. Extragalactic science emerged as one of the strong points of the survey. NOAO is the partner for data storage and access through its data archive program.

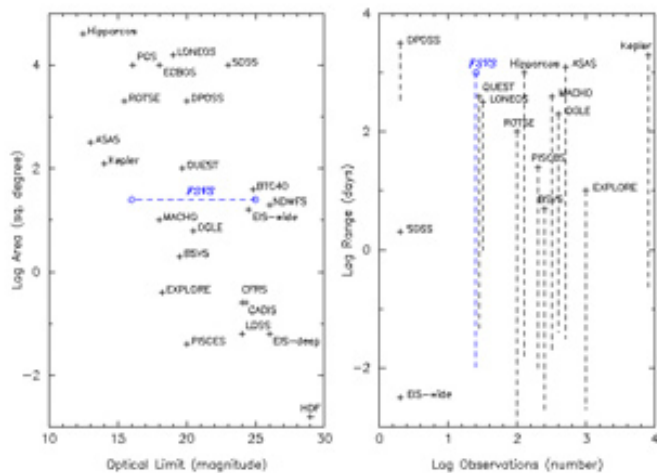


Figure 1. A comparison in area and depth between current major surveys and the FSVS. Adapted from the National Optical Astronomy Observatory (NOAO) Deep Wide-Field Survey Web pages (see [www.naoa.edu/naoa/naoadeep/](http://www.naoa.edu/naoa/naoadeep/)): SDSS, Sloan Digital Sky Survey (York et al. 2000); EIS (deep), ESO Imaging Survey (Deep) (Nonino et al. 1999); Deeprange, (Postman et al. 1998); INT-WAS, INT Wide Angle Survey (McMahon et al. 2001); HDF, Hubble Deep Field (Williams et al. 1996); NOAO, NOAO Deep-Wide Survey (Jannuzi & Dey 1999); CFRS, Canada France Redshift Survey (Lilly et al. 1995); CADIS, Calar Alto Deep Imaging Survey (Hippelein et al. 1998); CFDF, Canadian French Deep Fields (Brodwin, Lilly & Crampton 1999); LDSS, Low Dispersion Survey Spectrograph (Glazebrook et al. 1995); OGLE Optical Gravitational Lensing Experiment (Udalski et al. 1992). Note that most of these surveys have very limited or no variability information. The range in depth for the FSVS corresponds to using each individual image (as in the variability study) or the sum images. (From Groot et al. 2003)

Irene Barg and Phil Warner at NOAO were the archive architects for this survey.

The FSVS covered 79 fields at mid to high galactic latitude (and all right ascensions) to determine their content and variability. Magnitude ranges in each field are from about 16 (saturation) to 24 per exposure, with all variability information obtained in the V bandpass. Figure 1 shows the relationship of the FSVS survey to other well-known surveys. The limiting magnitude range of the FSVS is shown for a single image, or for a summed image over the V time-series sequence. The other surveys shown all have limited or no variability information.

The goal of the FSVS was the discovery and characterization of both photometrically and astrometrically variable sources in each field. Target astronomical objects were close binaries, RR Lyrae stars, rotational periods of active stars, solar system objects, optical transients such as GRBs, solar neighborhood stars, and Kuiper Belt objects. A number of other targeted programs have since made use of the data. To the magnitude depths of the FSVS survey, the sample of variable sources probes a large volume that will be populated by various interacting binaries, and will reach variables at the end of the main sequence (e.g., new CVs and late M- to early L-type dwarfs have been spectroscopically confirmed, and many W UMa stars identified via their phased light curves).

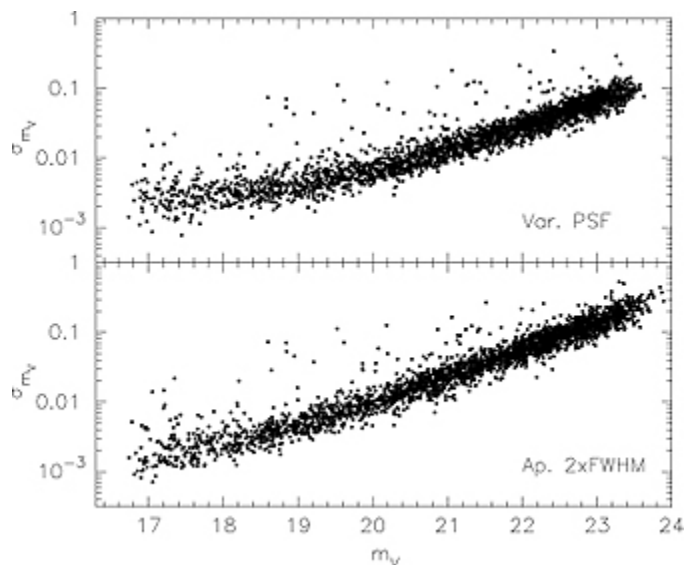


Figure 2. The standard deviation of the total light curves for point sources in a representative FSVS field. The top panel shows results using a variable PSF fitting routine to match seeing, while the bottom panel shows the results using aperture photometry with a fixed 2-arc-sec seeing FWHM aperture. (From Groot et al. 2003)

continued

Wide-Field Survey Reveals the Variable Sky continued

The multi-epoch observations in the FSVS consist of 10–30 V images in each field, spanning temporal sampling of 10 minutes over a single night to a log spacing over a week or so, and a final follow-up of each field one year later. Photometry was performed on each point source in each frame, and light curves were produced for approximately one million objects. B-V and V-I colors were determined as well, and we found a number of drop out sources, i.e., sources missing a single color due to faintness. Figure 2 shows our photometric results for a representative FSVS field.

Variability

The FSVS point source selection is formally greater than 90% complete (to V=22) with small galaxies, seeing, and blends being the largest confusion sources. Our light curves are sensitive to amplitudes as small as ~0.015 in V, and we can determine good periods over the range of one day or less from the V band observations. The fraction of point sources found to be variable is 5–8% in the V=17-22 range, and at least 1% are variable down to V=24. About 50% of all variable sources show variability on time scales of less than six hours. Brighter than V=19, the dominant population is low amplitude (< 0.05 mag), blue sources with apparently random variations. These sources are probably pulsating sources such as gamma Doradus or SX Phe stars. One-third of the short time scale variable sources are not detected in either B and/or I bands. Studies of the variable population using cuts of color, brightness, galactic latitude, and the like have been performed. Examples are shown in figure 3, and an example W UMA light curve is presented in figure 4.

Extragalactic Studies

The large area, depth, and colors of the FSVS have made it ideal for searches of galaxy clusters. Our FSVS collaborators Roger Clowes (University of Central Lancashire) and Ilona Soechting (Oxford) used the FSVS images to discover nearly 600 new galaxy clusters covering a wide range in richness, and spanning 0.05 to 0.9 in redshift. Over 100 of the clusters are at  $z > 0.6$ , and this new sample represents a significant addition to the currently known sample. These clusters are now being used to study quasar environments and the chemical evolution of galaxies. The FSVS cluster catalogue can be accessed at [www-astro.physics.ox.ac.uk/~iks/FSVScatalogue/home.html](http://www-astro.physics.ox.ac.uk/~iks/FSVScatalogue/home.html).

NOAO Data Archive

Reduced images and light curves for all point sources in the FSVS survey are now available via the NOAO Science Archive at [archive.noao.edu/nsa/](http://archive.noao.edu/nsa/). The archive also lists the most relevant published references to the survey, giving details of the data collection, reduction, and results to date.

We would like to thank Irene Barg for her significant contributions to the FSVS archive project. 

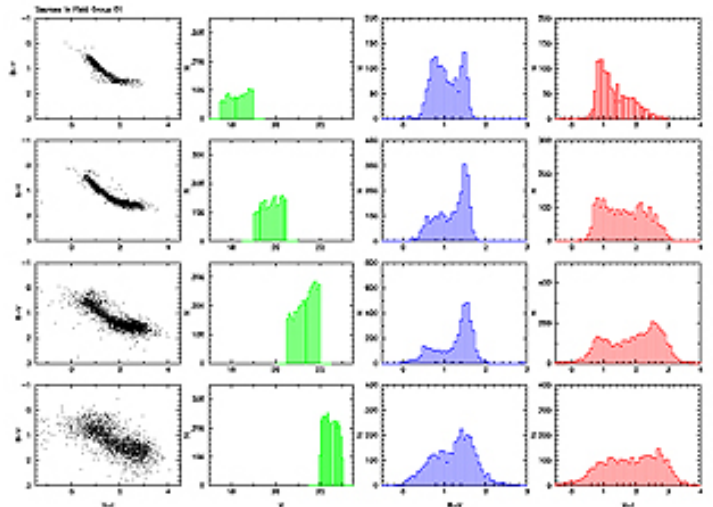


Figure 3. Color space in FSVS field 1 divided into V magnitude groups: V = 17.5–19.0, 19.0–20.5, 20.5–22.0, and 22.0–23.0 mag histograms are shown on the right as a function of V magnitude and color. (From Huber et al. 2006)

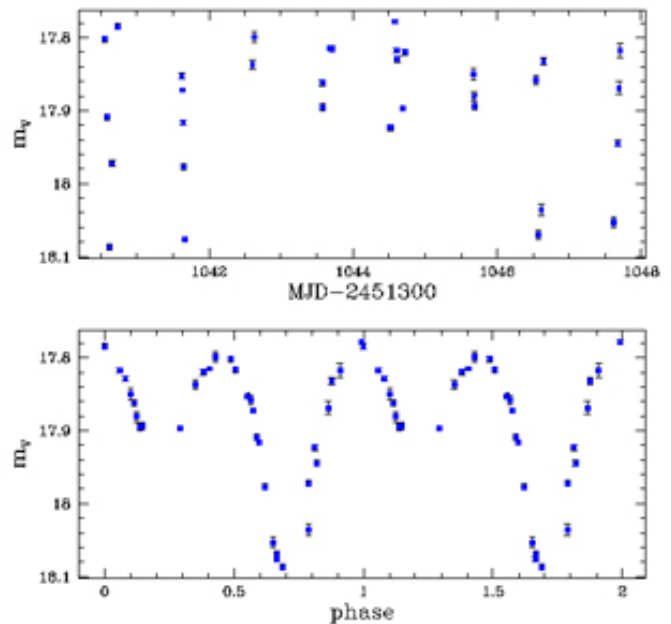


Figure 4. A sample variable (RR Lyrae) light curve from the data set, illustrating the typical time sampling for a field over a week-long timescale. Many fields will also have re-observations after 1-3 years.

# A New Component of the Solar Magnetic Field

Jack Harvey, Detrick Branston, Carl Henney (NSO), Christoph Keller (Utrecht University),  
& the SOLIS and GONG Teams

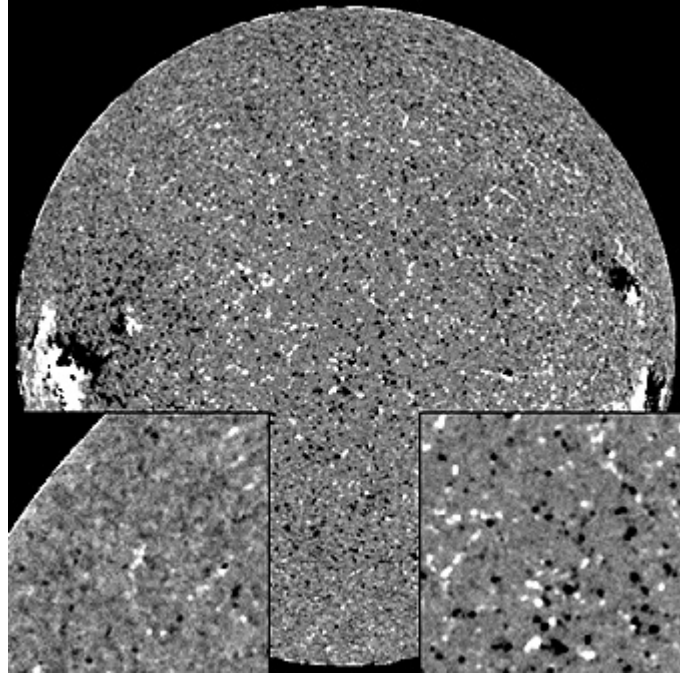
The solar magnetic field is not only the driver of solar activity, but is also a rich source of discovery about the behavior of magnetism throughout the cosmos. Since the first maps of the Sun's magnetic field were made 55 years ago, much has been learned about its structure and dynamics. Several components of the field have been defined in the solar photosphere, where observations of the Zeeman effect readily indicate the strength and orientation of the field.

The strongest field strengths (up to 6 kG) are found in dark sunspots. The umbral field is more or less vertically oriented, while the penumbra has a complicated structure with components that are nearly horizontal as well as ones that are inclined at moderate angles to the solar surface. The next most obvious magnetic components are fields in the vicinity of sunspots that comprise an active region. These fields are 1–2 kG and have a wide range of orientations. Outside of active regions, magnetic flux tends to be concentrated by convective downflows into a network of vertically-oriented, kilogauss-strength structures resembling flux tubes and flux sheets called the network field.

Some thirty years ago, an “internetwork” (IN) field component that is present everywhere in the otherwise quiet Sun was discovered in observations made at the McMath-Pierce Solar Telescope. The IN field consists of arcsec-sized flux elements that remain visible for an hour or so and frequently move as if entrained in convective flows. Because these features are small and do not contain much magnetic flux, they are hard to observe. Little is known about their intrinsic strength or orientation. Observations at the McMath-Pierce a few years ago suggested that there might be two components of the IN field: the relatively strong, mainly vertical-oriented component and a weaker, more nearly horizontal component. However, the observations were not conclusive.

With the advent of the SOLIS vector spectromagnetograph and recent improvements to the GONG magnetogram capability, we have new tools to observe the solar magnetic field with higher sensitivity and rapid cadence. Observations with both facilities show that everywhere outside of active regions, there is a nearly horizontal magnetic field that changes rapidly in time. In movies, it looks like a seething pattern of mottling. We find the orientation to be nearly horizontal because this unrecognized component is most prominent near the limb in measurements of the line-of-sight component of the magnetic field.

Correcting the observations for instrumental noise indicates that the field is inclined on average by about  $74^\circ$  to the local vertical. With our spatial resolution of a few arcsec, the (rapidly varying) field strength is about 1.7 G. With higher spatial resolution, the field would almost certainly be measured as stronger.



The line-of-sight component of the photospheric magnetic field observed with GONG (dark and light indicate away and toward field orientation). Insets are twice magnified sections from the upper left (left) and disk center (right). The newly observed component of the field is seen as mottling near the limb and is much weaker near disk center (being dominated there by the mixed polarity network and barely resolved IN fields). Movies show relatively slow evolution near disk center and rapid fluctuations near the limb.

The significance of this previously overlooked field component is not yet clear. Although inclined to nearly horizontal, the seething component contains significant magnetic flux. A simple calculation indicates  $3 \times 10^{22}$  Mx. This is equivalent to a large active region but is less flux than is present in the network.

Until we know the true field strengths and height variations, the energy content and power production in the dynamic field remain unknown. The seething field is uniformly distributed, which suggests a local origin probably related to convection. More details have been published in the *Astrophysical Journal Letters*, volume 659, page L177 (2007).

# The Solar Oxygen Crisis

Hector Socas-Navarro (*High Altitude Observatory*) & Aimee A. Norton (*NSO*)

Oxygen is the third most abundant chemical element in the Universe. In the past few years, new research indicates that the well-accepted value for solar oxygen abundance should be lowered. This has sparked controversy and created a “solar oxygen crisis.”

Prior to the new results, the solar oxygen abundance was assumed to be well-determined because a decade of results from helioseismology—the science of using sound waves to probe the solar interior structure and dynamics—agreed phenomenally well with theoretical models using the traditional value. If the oxygen abundance is revised (along with cascading effects on nitrogen, carbon, and neon), a thorough reworking of the solar sound speed profile and the solar interior model is needed.

The traditional value of the logarithmic oxygen abundance ( $\log \epsilon_{\odot}$ ) was 8.93 dex (with the astrophysics convention that  $\log \epsilon_{\text{H}} = 12$ ). Hydrodynamic simulations of solar granulation in 2004 by Martin Asplund and collaborators advocated lowering the oxygen abundance a factor of two to 8.66 dex. The new value presented the advantage of a better fit of the solar chemical composition within its galactic environment, since stars similar to the Sun have abundances lower than the traditional solar value. However, the lower abundance value was contradicted in 2006 by results from a 1-D semi-empirical model based on observations in CO bands, suggesting a value of 8.85, more consistent with the traditional view.

We decided to contribute to the debate by obtaining new observations that were spatially resolved and could account for the magnetic influences in the solar atmosphere. The new Spectro-Polarimeter for Infrared and Optical Regions (SPINOR) instrument was ideal to explore this topic. In October 2006, clear skies at the NSO/Sacramento Peak Dunn Solar Telescope allowed us to obtain a high-resolution (0.7 arcsec) map of the solar photosphere. For each pixel, we recorded spectro-polarimetric information for two magnetically sensitive Fe I lines and an O I triplet. The results were surprising.

Figure 1 shows a composite image of the temperature and magnetic flux density as derived from the SPINOR data. The cool

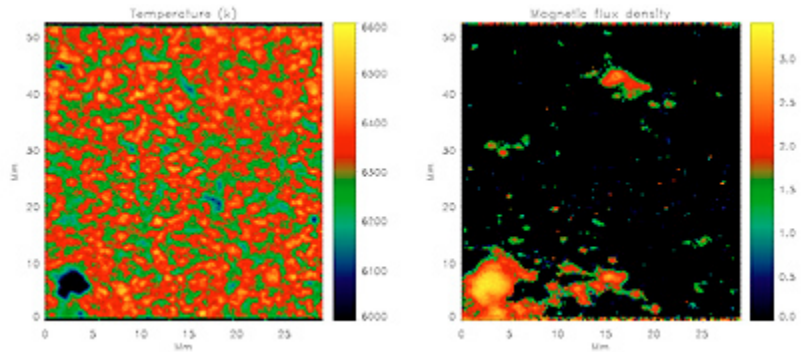


Figure 1. Maps of the temperature (left) and magnetic flux density (right) as derived from the SPINOR data.

feature in the lower-left corner is a ‘pore’—an area whose magnetic field is strong enough to block the heat of convection but is not as large and developed as a sunspot. The pore was used as a feature that the adaptive optics could lock onto in order to stabilize the image, allowing us to achieve the spatial resolution shown in the image. We obtained a 3-D model from inverting the Fe I lines to derive the vertical stratification of temperature, density, line-of-sight velocity and longitudinal magnetic field.

The oxygen abundance was determined independently at each pixel of the map, using the model atmosphere from the Fe I inversion and accounting for magnetic fields where appropriate. We employed both a local thermodynamic equilibrium (LTE) and non-LTE approach to the radiative transfer. The spatial distribution of  $\log \epsilon_{\odot}$  obtained with our 3-D semi-empirical model is shown in figure 2.

There is a variation of  $\log \epsilon_{\odot}$  over the map due to fluctuations in the solar atmospheric con-

ditions. Notice that the pore has considerably higher abundance than average. In general, magnetic concentrations exhibit higher abundances. We know of no physical reason why the abundance should show spatial variations in the solar atmosphere. We suspect the variations are caused by imperfect modeling of the atmosphere, especially in the presence of magnetic fields. This also implies that previous abundance determinations could have been biased by solar activity.

The mean values over the entire field of view are  $\log \epsilon_{\odot} = 8.94$  (LTE) and  $\log \epsilon_{\odot} = 8.64$  (non-LTE), with uncertainties of  $\sim 0.1$  dex. If we restrict the analysis to pixels with less than 100 Gauss of magnetic flux density, we obtain  $\log \epsilon_{\odot} = 8.93$  (LTE) and  $\log \epsilon_{\odot} = 8.63$  (non-LTE). The non-LTE value should be the one most applicable to the solar atmospheric conditions, and its value advocates for a downward revision of the oxygen abundance, in agreement with the simulations from 2004.

See Socas-Navarro and Norton, 2007, *ApJ*, 660, L153 for more detailed information.

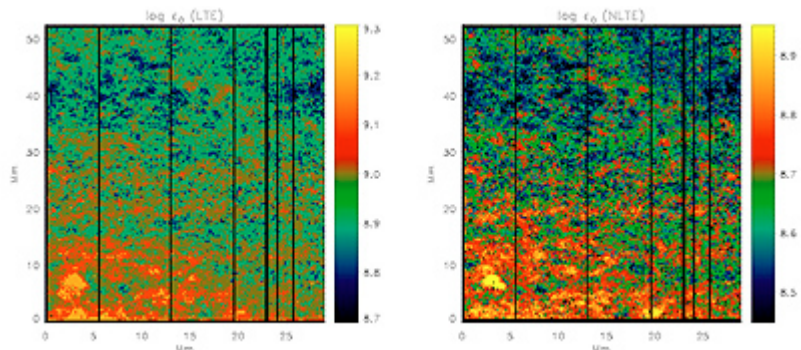


Figure 2. The logarithmic oxygen abundance as determined from LTE (left) and non-LTE (right) calculations.

# Disturbing News in the Large Magellanic Cloud

*Knut Olsen*

The Large Magellanic Cloud (LMC), one of the nearest and most famous galaxies in the sky, is invaluable for its use as an astrophysical laboratory. The LMC is a critical calibrator of the extragalactic distance scale, it serves as the background source in many of the hunts for galactic-halo dark matter through microlensing, and it provides the most accessible environment in which to study the effects of lower metallicity on star formation and the interstellar medium. For all of these distinct purposes, a clear understanding of the LMC's global structure and dynamics is very important.

In October 2001, Phil Massey (Lowell Observatory) and I used the Cerro Tololo Inter-American Observatory (CTIO) Blanco 4-meter telescope and Hydra-CTIO fiber spectrograph to obtain spectra of 167 LMC red supergiants (RSGs), and an additional 118 RSGs in the Small Magellanic Cloud (SMC). Our primary goal was to observe the effect of low metallicity on the properties of the RSGs and compare them with stellar evolutionary predictions (see Massey & Olsen 2003).

At about the time that these observations were collected, van der Marel et al. (2002) completed a comprehensive analysis of the dynamics of the LMC's carbon stars, finding a rotation curve with a significantly different dynamical center and lower amplitude than previous studies, notably those based on HI gas observations (Kim et al. 2001). Thus, our second goal was to compare the LMC's young stellar kinematics, as traced by the RSGs, with that of the older carbon stars and the HI gas.

Our analysis of the LMC's kinematics, which appeared in the *Astrophysical Journal Letters* in February, found some surprising new results. These findings were only made evident by first combining the RSG, carbon star, and HI samples, and then accounting for the most recent accurate measurement of the LMC's proper motion (Kallivayalil et al. 2006). Because the LMC spans a large portion of the sky, its transverse motion imparts a line-of-sight velocity gradient that, left uncorrected, masks the LMC's internal kinematics; Kallivayalil et al. (2007) found that the LMC's space motion is faster than previously thought.

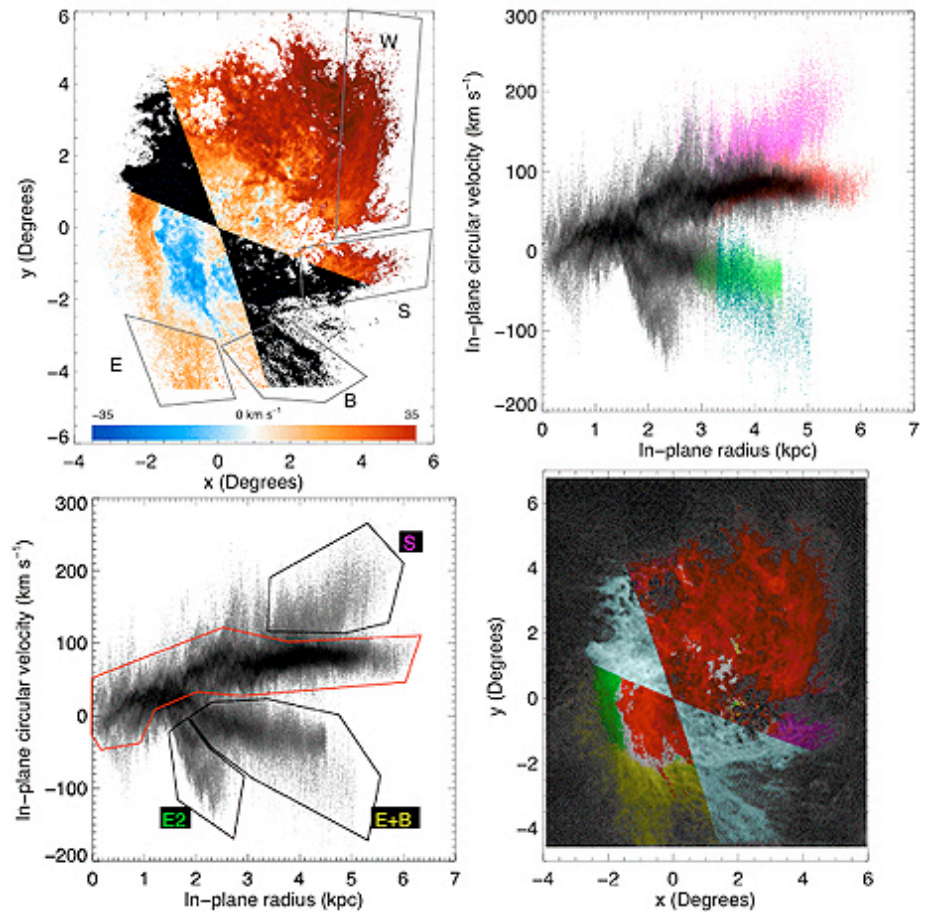


Figure 1. Kinematic signatures of the LMC's HI. Top left: The emission-weighted velocities from the ATCA+Parkes HI survey (Kim et al. 2003), minus the contribution from the LMC's space motion (Kallivayalil et al. 2006), are shown (in color in the electronic version of this Newsletter at [www.noao.edu/noao/noaonews.html](http://www.noao.edu/noao/noaonews.html)), along with regions marking the locations of previously identified HI tidal arms. The black bowtie-shaped region was excluded from the analysis. The velocity scale runs from  $-35 \text{ km s}^{-1} < v < 35 \text{ km s}^{-1}$ ; north is up and east to the left. The origin is fixed to the dynamical center derived from the carbon stars, while the image is projected onto the tangent plane. Top right: The velocities shown at left have been converted to in-plane circular velocities and are plotted vs. in-plane radius. Data points belonging in each of the boxes at left are shown in different colors, as follows: arm W in red, arm S in magenta, arm B in cyan, and arm E in green. Bottom left: We identified four regions with distinct kinematic signatures. The red box outlines the main LMC rotation curve and encompasses arm W. The others are a region with velocities like those of arm S, a region containing arms E and B, and a new feature with distinct kinematics that we label E2. Bottom right: The HI gas contained within the regions drawn at bottom left are plotted with different colors as follows: red for the main rotation curve, magenta for the arm S region, yellow for the combined arm E and B regions, and green for region E2. Figure and caption reproduced from Olsen & Massey (2007).

Using a solution of the carbon-star kinematics as a common reference point, we looked for the signatures of internal rotation and other motions in the LMC's HI, carbon stars, and RSGs. In the HI, Staveley-Smith et al.

(2003) had previously identified arms of gas that appeared to be connected to larger-scale HI tidal features, such as the Magellanic Bridge and Magellanic Stream. Figure 1 shows that these arms clearly stand out in our


*continued*

*Disturbing News in the LMC continued*

analysis. We also found an additional body of gas that appears to have a tidal origin, and showed that the HI that traces the LMC's internal rotation is elliptical in shape and significantly asymmetric around the carbon-star dynamical center.

Comparing the carbon star kinematics with that of the HI (see figure 2), we found that many of the carbon stars on the periphery of the LMC have velocities and spatial distributions that associate them with the HI tidal arms. This is the first evidence of disturbed stellar kinematics in the LMC, and suggests that many more stellar velocities will be needed to decipher the LMC's internal kinematics and define its gravitational potential. The RSGs, by contrast, are entirely confined to the region of HI gas that traces the LMC's rotation. This means that the tidal arms formed longer than ~50 Myr ago, and that no star formation has occurred in them.

Our results fit well with the general picture of a tidally disturbed LMC that has been developed over the past few years through studies of the galaxy's geometrical structure. These studies have found that the LMC's disk is elongated (van der Marel 2001, van der Marel & Cioni 2001) and has significant out-of-plane structure (Olsen & Salyk 2002, Nikolaev et al. 2004), all attributed to the gravitational influence of the Milky Way and SMC.

The only problem with the internal consistency of this picture stems from the same proper-motion measurement on which the dynamical analysis is based. The proper motion measured by Kallivayalil et al. (2006) is so large that it appears that the LMC is not gravitationally bound to the Milky Way (Besla et al. 2007), meaning that the Magellanic Clouds are passing by our galaxy for the first time, leaving minimal opportunity for the Milky Way to inflict heavy damage on the LMC. We clearly have much to learn about one of our nearest neighbors! 

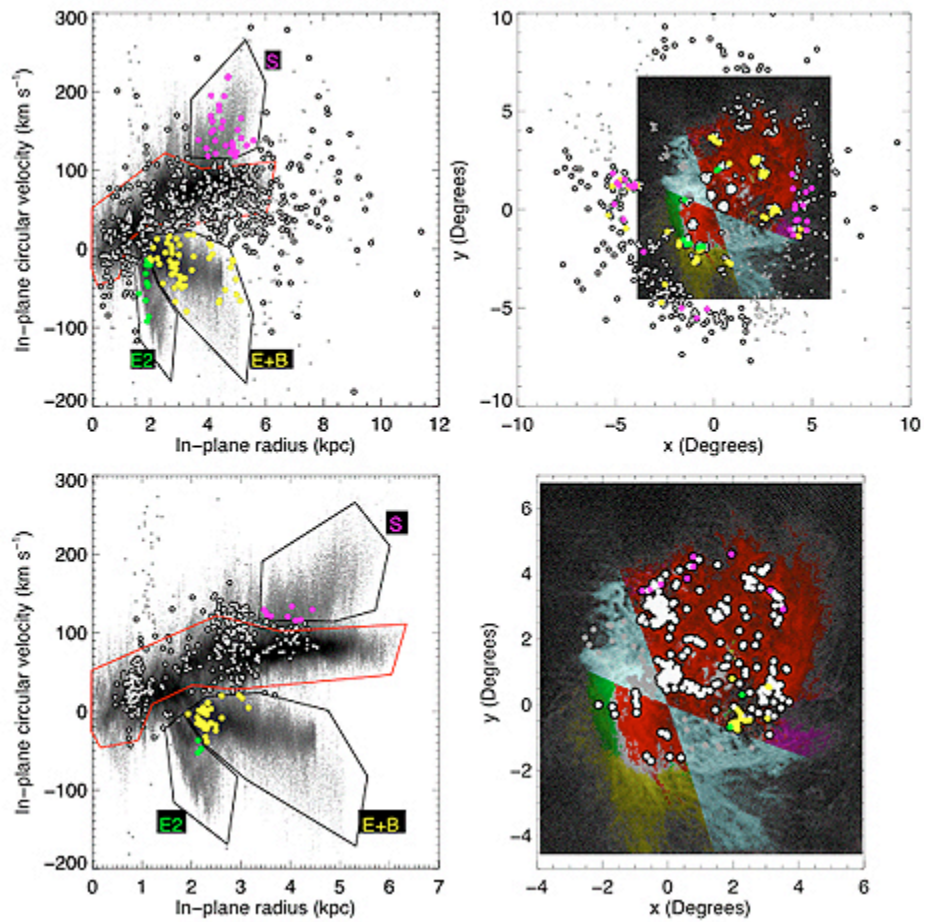


Figure 2. Comparing the LMC's stellar kinematics to that of the HI (for color figure, see the electronic version of this Newsletter at [www.noao.edu/noao/noaonews.html](http://www.noao.edu/noao/noaonews.html)). Top left: As in figure 1, the line-of-sight HI velocities converted to in-plane circular velocities are shown vs. in-plane radius; the distinct kinematic regions from figure 1 are also reproduced. Overplotted as circles are the carbon star velocities. Carbon stars falling within the regions S (magenta circles), E+B (yellow circles), and E2 (green circles) are labeled in color. The small gray points are carbon stars falling in the excluded region where in-plane circular orbits are nearly perpendicular to the line of sight. Top right: The positions of the carbon stars and HI on the sky are shown, with symbols and color labels for the carbon stars as on the left and as in figure 1 for the HI. Many of the carbon stars that have kinematics like that of the tidal HI arms are also spatially coincident with those arms, implying physical association. Bottom panels: Comparing the red supergiant kinematics to that of the HI. Symbols and colors are as in top panels. The RSGs are all confined to the HI region that traces the LMC's rotation. Figure and caption reproduced from Olsen & Massey (2007).